UNIVERSITÀ DI PARMA
ARCHIVIO DELLA RICERCA

University of Parma Research Repository

Deep and shallow electronic states associated to doping, contamination and intrinsic defects in ε-Ga2O3 epilayers

(Article begins on next page)

12 October 2022

Deep and shallow electronic states associated to doping, contamination and intrinsic defects in ε-Ga$_2$O$_3$ epilayers

Antonella Parisini[1]*, Alessio Bosio[1], Hans Jurgen von Bardeleben[2], Juan Jimenez[3], Shabnam Dadgostar[3], Maura Pavesi[1], Andrea Baraldi[1], Salvatore Vantaggio[1], Roberto Fornari[1,4]

[1] University of Parma, Dept. of Mathematical, Physical and Computer Sciences, Parco Area delle Scienze 7/A, 43124 Parma, Italy

[2] Sorbonne Université, Institut des Nano-Sciences de Paris (INSP) 4, Place Jussieu, 75005 Paris, France.

[3] University of Valladolid, Dept. of Condensed Matter Physics, Paseo de Belén 19, 47011 Valladolid, Spain

[4] IMEM-CNR, Institute of Materials for Electronics and Magnetism, Parco Area delle Scienze 37/A, 43124 Parma, Italy

ABSTRACT Deep and shallow electronic states in undoped and Si-doped ε-Ga$_2$O$_3$ epilayers grown by MOVPE on c-oriented Al$_2$O$_3$ were investigated by cathodoluminescence, optical absorption, photocurrent spectroscopy, transport measurements, and electron-paramagnetic-

resonance. Nominally undoped films were highly resistive, with a room temperature resistivity varying in the range 10^7- 10^{13} Ωcm depending on the carrier gas used during growth. Films grown with He carrier were generally more resistive than those grown with H_2 carrier and exhibited a Fermi level located at about 0.8 eV below the conduction band edge, which tends to shift deeper with temperature. This can tentatively be attributed to the combined action of deep donors (probably carbon impurities and oxygen vacancies) and deep acceptors (Ga vacancies and related complexes), which compensate residual shallow donors. There are strong experimental hints that nitrogen also behaves as deep acceptor.

Room temperature resistivity as low as 0.42 Ωcm and electron concentrations around 10^{18} cm^{-3} were obtained by silicon doping. Si was confirmed to act as shallow donor with sufficiently high solubility. A variable range hopping conduction was observed in a wide temperature interval in the *n*-type layers, and compensation by native acceptors also plays a major role on conduction mechanisms. Previous evaluations of curvature and anisotropy of the conduction band are confirmed, which allows for the estimation of the electron effective mass.

The present experimental data are discussed considering the theoretical predictions for point defect formation in the ε-polymorph as well as literature data on extrinsic and intrinsic defects in β-Ga_2O_3.

One Sentence Summary. Shallow and deep electronic defects detected in highly resistive and highly conductive ε-Ga_2O_3 thin films and survey of literature data.

Introduction

Ga$_2$O$_3$ is a wide-bandgap semiconductor with physical properties suitable for application in power electronics, short wavelength photonics, gas sensors, and spintronics [1-5]. The monoclinic β-phase is the only one thermodynamically stable among the five polymorphs α, β, γ, δ, and ε. Its bandgap of nearly 5 eV enables transparency up to the UV-C spectral range; however, the crystalline structure favors undesired cleavage, especially along (100) and (001) directions, and is responsible for the anisotropy of thermal, vibrational and optical properties [6,7].

ε-Ga$_2$O$_3$ is the second most stable polymorph, identified by Playford et al. in 2013 [8]. Its crystalline lattice was found to be orthorhombic and stable up to about 700°C, but it was seen to convert to monoclinic β at 900°C [9]. A peculiarity of ε-Ga$_2$O$_3$ is its ferroelectric behavior [10], connected with a spontaneous polarization of the lattice that might turn out useful to produce a two dimensional electron gas at the interface with other compounds, such as CaCO$_3$ [11]. When deposited on hexagonal (0001) sapphire, the epitaxial ε-Ga$_2$O$_3$ films arrange in domains, 5-10 nm in size, separated by 120° twins. On average, this ordering results in a pseudo-hexagonal structure, with the c-axis aligned to the c-axis of the substrate, and an ABAC 4H stacking sequence, where Ga atoms occupy octahedral and tetrahedral sites in between oxygen planes, leaving a certain number of empty sites to ensure the 2:3 stoichiometric ratio [10,12]. Two kinds of layers alternate in the orthorhombic cell of *ε*-Ga$_2$O$_3$ (Fig.1): layers containing only octahedral sites (Ga1 and Ga2), and layers where Ga atoms occupy both octahedral (Ga3) and tetrahedral (Ga4) sites. Anti-phase boundaries are often observed inside the domains [10].

The epitaxial growth of ε-Ga$_2$O$_3$ takes place at relatively low temperature of 600-650 °C, lower than the one usually employed for the β-phase. The first successful attempt to grow epitaxial layers

of this polymorph dates back to 2015, with the pioneering work by Oshima [13], who deposited

pure ε-phase epilayers on hexagonal GaN and AlN substrates by Hydride Vapour Phase Epitaxy

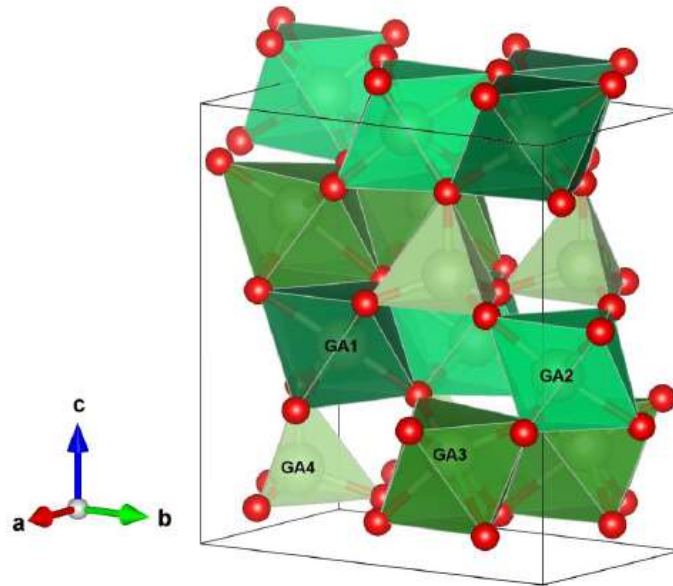(HVPE). Subsequently, thin films have been grown on c-sapphire and 6H-SiC by Metal-Organic

Fig.1 ε-Ga_2O_3 crystalline structure: gallium ions (green balls) and oxygen atoms (red balls) [10].

Four non-equivalent Ga sites are labelled: Ga1 and Ga2 are in layers containing only octahedral sites;

an octahedral Ga3 site and a tetrahedral Ga4 site are in the adjacent layers.

Vapour Phase Epitaxy (MOVPE) respectively by Boschi et al. [14] and Xia et al. [15] and later by

Yao et al. [16]. Other methods also proved to be successful: mist-Chemical Vapour Deposition

(CVD) [17-19] and plasma assisted Molecular Beam Epitaxy (MBE) [20]. In the latter case, using

tin or indium as metal catalysts, above a critical concentration, which permits to stabilize the ε-

phase of Ga_2O_3 with respect to the β-phase. The control of the HCl flux in MOVPE growth has

been demonstrated to be decisive to control the dominant phase among α, β or ε [21]. Chlorine and

hydrogen are supposed to work as catalyst to promote and stabilize the ε-phase formation. The

critical conditions for the preferential nucleation, in a MOVPE deposition, of the ε-phase on Al_2O_3, instead of the β-one, have recently been discussed in Ref. [22]. Low temperature and small layer thickness have been also demonstrated to favour ε vs β-phase in MOVPE growth [23]. The deposition parameters leading to the stabilization of different Ga_2O_3 polymorphs have been recently reviewed by Bosi et al. [24].

The growth conditions and the structural properties of ε-Ga_2O_3 are relatively well known, however its electronic properties and defects are still quite unknown. A very flat valence band (VB) and a pronounced conduction band (CB) minimum at the Γ point, as in β polymorph, have been reported in Refs. [25,26] as deduced from angular resolved photo-electron spectroscopy (ARPES) and density functional theory (DFT) calculations. An effective mass of about 0.3 m_e with negligible anisotropy around Γ point has been recently deduced from electron paramagnetic resonance (EPR) data [27]. This result has been supported by a calculated value of 0.24 m_e [28]. In the latter work, the piezoelectric properties of the crystal have also been discussed, consistently with both the prediction of a large spontaneous polarization of ε-Ga_2O_3 [29], and the experimental detection of ferroelectric hysteresis [12]. The bandgap of ε-Ga_2O_3 was reported to be in the range 4.6-4.9 eV at room temperature (RT) [13,30], close to the bandgap of β-Ga_2O_3, a value that makes ε-Ga_2O_3 suitable for UV-C detector fabrication [30].

First information on electrical properties and photoconductivity (PC) of as-grown nominally undoped (UD) ε-Ga_2O_3 was reported in Ref. [30] for layers deposited by MOVPE on (0001) sapphire using He as a carrier gas. A thermally activated conductance behavior characterized by an activation energy of about 0.7 eV was found in the highly resistive samples. Ref. [30] also reports the first evidence of deep levels in the ε-phase, suggested by a non-negligible photoconductive response to sub-bandgap energy photons, and confirmed by the broad

cathodoluminescence (CL) emission in the spectral range 2.4-3.2 eV [31]. Such a broad CL band was observed to have shape and intensity weakly sensitive to carrier gas, but strongly dependent on measurement temperature between 80 K and 300 K. RT CL emission in the range 1.5-4.2 eV has been more recently reported in Ref. [32], where a shoulder at about 1.65 eV was also evidenced.

Deep levels related to intrinsic defects such as O and Ga vacancies, interstitials and/or their complexes are probably formed in ε-Ga$_2$O$_3$, as formerly proposed for the β-polymorph [33,34]. The formation of some complexes (e.g. V_{Ga}-Ga_i-V_{Ga}) has been experimentally confirmed by EPR investigation in irradiated β-Ga$_2$O$_3$ [35,36]. A comparison between the electronic properties of the Ga$_2$O$_3$ polymorphs is given in Ref. [37].

Successful n-type conductivity by Si and Sn doping has been demonstrated [27,38], with the carrier transport taking place via localized states, as inferred from Hall effect and EPR investigations. The effect of Si-doping on the CL emission, as well as the effect of the carrier gas (H$_2$, He and N$_2$) in the MOVPE growth have been discussed in Ref. [31]. On the contrary, an effective p-type doping was never achieved; the predicted hole self-trapping energy of ε-Ga$_2$O$_3$ being even higher than in β-Ga$_2$O$_3$ [39], which implies formation of polarons instead of free holes [40].

The present work reports on electrically and optically active point defects in ε-Ga$_2$O$_3$ and associated electronic states in both nominally undoped resistive and n-type ε-Ga$_2$O$_3$ layers. New measurements provide new insight into nominally undoped ε-Ga$_2$O$_3$ samples, which were previously investigated by other methods. This allows to establish a correlation of all available experimental results. The nature and activity of intra-gap states in ε-Ga$_2$O$_3$ were investigated by several experimental methods, i.e. CL, absorption and photocurrent spectroscopy, transport

measurements and EPR investigations. The new experimental findings of the present work are discussed in the light of Refs. [25,27,30,31,38] and considering theoretical estimates and previous results relevant to β-phase.

All ε-Ga_2O_3 samples investigated in this paper were grown by MOCVD, using He, H_2 or N_2 carrier gases, following the process described in [14]. For the first time, the influence of the carrier gas on electrically-active defects is discussed. UD samples grown with He as a carrier gas exhibited higher dark resistivity with respect to those grown with H_2, and appeared to be suitable for photo-detection of UV-C radiation. On the other hand, non-equilibrium occupancy of deep defects in UD and Si-doped ε-Ga_2O_3 samples grown in H_2 are observed for the first time in this polymorph.

Heavily Si-doped samples are better grown with H_2 carrier gas, which opens the way to novel electronic devices based on *p-n* heterojunctions. The possibility of *n*-type doping ex-situ by Sn diffusion is also mentioned. Finally, we discuss about the effects of nitrogen incorporation in epilayers grown under N_2 carrier gas.

With the original results on the ε-Ga_2O_3 epilayers mentioned above, we updated the body of knowledge on deep and shallow levels detected in UD and *n*-type doped ε-Ga_2O_3 layers grown by MOCVD.

Experimental Section

The nominally UD samples studied in this work were grown at IMEM-CNR Institute by MOVPE under total pressure of 60 mbar on 2-inch c-plane sapphire substrates heated at either 600 °C, 610 °C, or 650 °C. He, H_2 or N_2 were used as carrier gas, and trimethylgallium (TMG) and ultrapure water were used as precursors for gallium oxide synthesis. Typical H_2O/TMG ratio was in the (100-350) range. The films were transparent and smooth [14], with layer thickness in the

range 0.2-0.5 μm. X-ray measurements confirmed the good quality of the layers and their single phase structure.

Silicon doping was achieved by adding silane to the precursors during growth. A mixture of 0.05% SiH_4 in pure H_2 was injected into the growth chamber to give an overall silane flow around 0.005 sccm [38].

The process parameters of the ε-Ga_2O_3 thin films here discussed are indicated in Table 1.

Fig.2 shows the (006) X-ray diffraction peak typical of both undoped and Si-doped ε-Ga_2O_3 layers compared to the (-603) peak of a bulk β-phase sample (by Novel Crystal Technology Inc.). Note the splitting of the diffraction peaks of both undoped and Si-doped films, due to Kα_1 and Kα_2 radiations of the anode, which indicates a high crystallographic quality; the comparison also
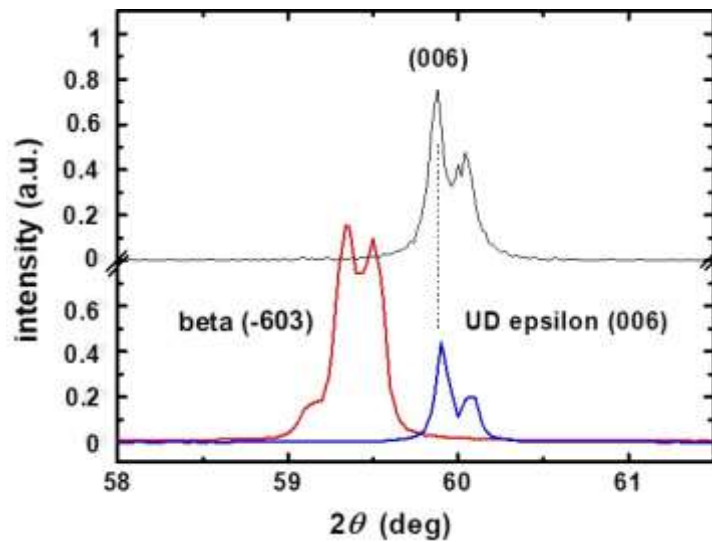

Fig.2 (006) X-ray peak of UD (blue line) and Si-doped (black line) ε-Ga_2O_3 layers in comparison with (-603) peak of a β-Ga_2O_3 (red line). The splitting of the diffraction peaks is due to Kα1 and Kα2 radiations of the anode.

confirms that Si incorporation during the epitaxial growth does not alter the crystallographic structure. Further details on X-ray investigation of these samples can be found in Refs. [9,27,31].

The resistivity measurements were performed by van der Pauw method on square 5×5 mm^2, doped samples with triangular or square contacts in their corners. A Keithley set-up for Hall and resistivity measurements was used. In case of highly resistive layers the Transfer-Length-Method (TLM) was preferred over the van der Pauw geometry or other standard 4-point probe methods, because of the shorter distance between the contacts, i.e. lower resistance (and lower compliance voltage). Five striped electrodes were deposited on the surface of the sample, previously etched in a solution of hydrofluoric and nitric acid (HF 50% + HNO$_3$ 50%) for 1 min and then rinsed in acetone, isopropanol and deionized water, and finally dried blowing dry nitrogen. The electrodes were 4 mm long and 0.45 mm wide, and the gap between adjacent contacts was 0.2, 0.4, 0.8 and 1.6 mm, respectively. A tolerance of about 5% on the distances between contacts was confirmed by optical microscopy. Current-voltage characteristics of each couple of adjacent electrodes were recorded with a Source-Meter Keithley (Mod. 2400) up to 200 V. The ohmic behavior was generally tested up to a temperature of 600 K.

The electrical contacts were made of Ti/Au double layers, deposited by thermal evaporation or sputtering, except for sample #440 (see Table 1), for which a SnO$_x$ layer was deposited by sputtering in order to locally dope the epilayer with Sn [38,41]. In all cases, the ohmic behavior of the contacts was tested in the whole temperature range of the electrical investigation.

The PC response of the UD film was recorded over a wide spectral range by RT photocurrent spectroscopy. An ORIEL 300 W Xenon lamp and a monochromator CornerStone 130TM 1/8 m (Mod. 74000) (spectral range 200 -1600 nm, wavelength resolution of 3 nm) were used. The results were corrected for the spectral emission of the lamp using a calibrated Newport 840-C Optical Power Meter. The bias dependence of the photoresponse was analyzed up to V=200 V. Optical

absorbance measurements (OAM) were performed at RT in the 200-800 nm range with a Varian 2390 spectrophotometer.

Table 1. Process parameters of the samples discussed in this work ([tw] is for "this work").

Samples # - SiH₄ flow (sccm)	T (°C) - P (mbar)	Carrier flow (sccm)	Carrier gas	O/Ga ratio	Time (min)	Thickness (nm)	Metal contact
#146 - **undoped** [tw], [9]	650 - 100	200	He	205	15	500	Ti/Au
# 425- **undoped** [31]	610 - 60	1000	H₂	350	320	6000	-
#479- **undoped** [31]	650 - 100	200	He	205	15	450	-
#307 - **0.005** [38]	600 - 60	1000	H₂	145	60	1000	Ti/Au
#335 - **0.005** [tw], [27,38]	610 - 60	1000	H₂	145	60	450	Ti/Au
#440 - **0.005** [tw]	610 - 60	1000	H₂	350	60	550	SnOₓ

EPR measurements were carried out from 4K to RT on selected Si-doped samples with a 6×4 mm² size by means of a X-band spectrometer (9 GHz) with 100 KHz magnetic field modulation and lock-in detection. The absolute spin concentration (spins/cm³) in the Si doped ε-Ga₂O₃ films was estimated at RT from the comparison with a spin standard sample (Al₂O₃: Cr), containing 9.2×10^{15} spins, as described in Ref. [27], and assuming a homogeneous distribution over the whole sample thickness. Further details on the EPR experiments are reported in Ref. [27].

CL measurements were carried out on the UD sample in the temperature range 80-300 K. The CL was measured with a MonoCL2 system from Gatan UK, attached to a field-emission scanning electron microscope (FESEM-LEO 1530). A Peltier-cooled CCD detector was used for the spectral

analysis, while the panchromatic spectra were recorded with a photomultiplier. More details about the experimental set-up and the CL response of the ε-Ga_2O_3 samples are reported in Ref. [31].

Results and discussion

In this section we first discuss the results obtained on undoped and Si-doped ε-Ga_2O_3, while at the end of the section we shall discuss the interplay between shallow donors and deep levels.

1. Undoped ε-Ga_2O_3

Nominally UD layers were found to be highly resistive regardless of carrier gas type. With H_2 carrier gas a RT resistivity of the order of 10^7 Ωcm was typical [31,38], while the use of He generally led to much higher resistivity. Values up to 10^8 Ωcm at 600 K, corresponding to an extrapolated RT value of about 10^{13} Ωcm, were found.

1.1 Role of native donors and H_2 incorporation in UD ε-Ga_2O_3.

Resistivity of UD samples (#146) grown with He carrier gas was evaluated by means of TLM measurements; this is the first measurement of the resistivity as a function of the temperature reported for ε-Ga_2O_3. Typical current-voltage curves for the four couples of electrodes are shown in Fig.3a: a linear ohmic behavior up to 200 V with slopes that scale with the distance d_i (i=1- 4) between the contacts is observed. The dependence of the resistance on the contact distance d_i at the temperature of 573 K is reported in Fig.3b, and from its slope a resistivity of about 10^8 Ωcm has been estimated. In principle, TLM measurements provide information on both specific contact resistivity and bulk resistivity of the semiconductor, if all contacts are considered identical.

However, the extrapolation to $d = 0$ of the line in Fig.3b gives an intercept close to zero with the vertical axis, indicating that in such sample the geometry of the pattern is not adequate to resolve the contact specific resistivity and the transfer length.
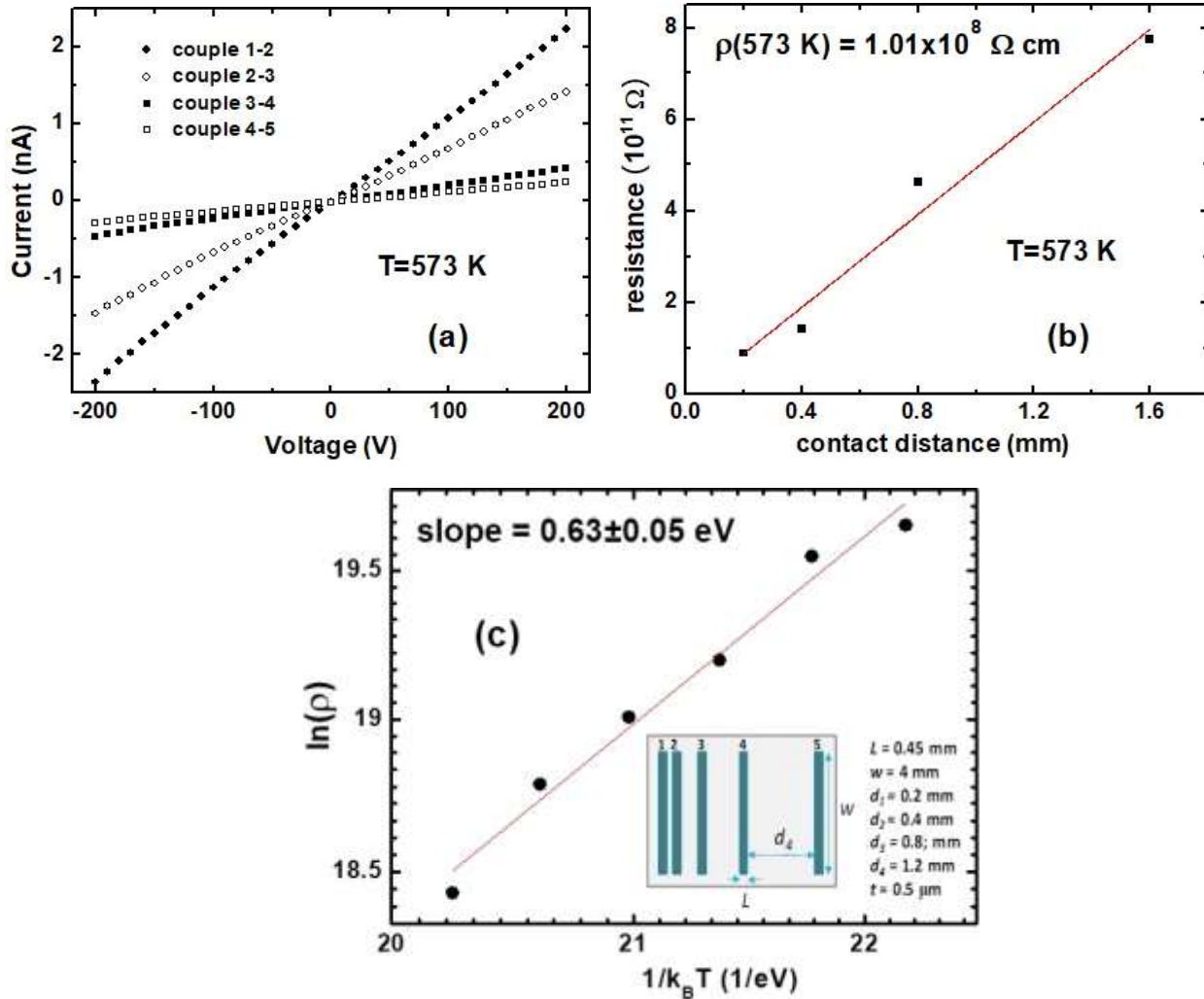

Fig.3 (a) Current-voltage characteristics at T=573 K for four couples of adjacent contacts (see TLM pattern in the insert of Fig 3c). (b) Total resistance at T=573 K of the four couples of contacts as a function of the intra-contact distance. (c) Arrhenius plot (k_B is the Boltzmann constant) of the bulk resistivity (in Ωcm) in a highly resistive sample, measured by TLM (in the insert: sketch of contact pattern).

Fig.3c shows the Arrhenius plot for the dark resistivity, as calculated from the slope of plots like those of Fig.3b, in the temperature range (523-573) K. Below 520 K the resistance of the sample exceeds the maximum value that can be measured by our experimental setup. Assuming a thermally activated electrical conduction mechanism, the extrapolation to RT of the resistivity data of Fig.3c leads to a value of the order of 10^{13} Ωcm, the highest value measured in our samples so far. On the other hand, the RT resistivity of films grown with H_2 carrier gas was generally of the order of 10^7 Ωcm [31,38]. The measure of the resistivity permits an evaluation of such a slope independently of the electrical contacts.

The activation energy of 0.63 eV obtained from the Arrhenius-plot agrees with the thermal activation energy of the conductance ($\approx$ 0.7 eV) previously reported for undoped ε-Ga_2O_3 grown by MOVPE using either He [30] or Ar carrier gas [42,43]. Notice that in Ref. 42 the data from RT to about 600 K confirm a conductance variation of about five orders of magnitude, which supports the value of resistivity extrapolated to RT from the data of Fig.3.

Because of the nearly flat VB structure [25,26], and the self-trapping of holes [37], electrical transport by electrons dominates over the possible hopping of self-trapped holes, therefore, the (0.6-0.7) eV activation energy is indicative of the Fermi level position with respect to the CB minimum E_c, i.e. the semiconductor is weakly n-type. This may be explained in terms of the thermal emission of electrons bound to deep donors, similarly to what estimated from the slope of conductance Arrhenius plot in Ref. [42]. That conclusion was based on the study of current-voltage characteristics in metal-semiconductor junctions in the high-electric-field regime. The I-V plot was interpreted in terms of Poole-Frenkel electron emission from defects, thus obtaining a 0.7 eV barrier height.

An approximated evaluation of the Fermi level position with respect to the CB in sample #146 is obtained calculating at first the electron density from the resistivity assuming an electron mobility (at any temperature) of about 10 cm^2/Vs. The effective density of the states of the conduction band can be estimated assuming an effective mass of 0.3 m_e [27], so that finally the Fermi energy results to linearly vary between ≈0.8 eV (at RT) and ≈1 eV (at about 600 K), with an extrapolated value at T=0 of 0.8 eV. Such a value is comparable to the thermal activation energy of the electrical conduction (Fig. 3).

The present data support the presence of unintentional deep donors in our samples and we shall now examine which defects may act as deep donors, starting from oxygen vacancies (V$_O$). These were first investigated in β−Ga$_2$O$_3$ [44] and were expected to behave as a negative-U center, with a (2+/0) transition level between 1.5 and 2.1 eV below the CB minimum in all Ga$_2$O$_3$ polymorphs [37]. Such a defect can certainly play a role in the control of the electrical properties in highly resistive ε-Ga$_2$O$_3$. At first sight, the oxygen vacancy can roughly justify the resistivity variation with temperature shown in Fig. 3 and of the conductance reported in Ref. [30]. However, this alone cannot explain the variation of the RT resistivity with the carrier gas, discussed in this work. This suggests that donor levels shallower than V$_O$ should be present and play an important role in terms of carrier release upon heating.

Carbon, unavoidably incorporated during the epitaxial growth with metal-organic precursors in a reaction chamber with graphite heater [45], might be considered as a possible additional donor defect, although its density and activation energy in ε-Ga$_2$O$_3$ have not yet unambiguously determined. Wei et al. discussed a PL emission at (0.6-0.7) eV in C-doped β-Ga$_2$O$_3$, attributed to C in Ga sites [46]. The role of carbon in different Ga$_2$O$_3$ phases has been theoretically discussed by Lyons et al. [47], while Lany [34] suggested that carbon on Ga site in β-Ga$_2$O$_3$ can introduce a

deep donor with negative-U character, with a level $E(+/-)$ at 0.81 eV below the CB. In this assumption, a distorted DX-like state should become energetically favorable in n-type conducting samples, where carbon can behave as either a donor, or as a compensating impurity depending on the Fermi level position, thus possibly leading to Fermi-level pinning, compensation, and persistent photoconductivity. A similar behavior can be expected for C in the ε-phase, considering the similarities in the energy states of impurities in all Ga_2O_3 polymorphs suggested in Ref. [37].

We observed that a conduction activation energy around 0.7 eV was reproducibly obtained in highly resistive samples grown by different MOVPE reactors, under different growth conditions and different carrier gas (He [30] or Ar [42]); therefore, the hypothesis of a conductivity controlled by an unintentional donor at about 0.7 eV from E_C is plausible, which well agrees with the Fermi level extrapolated at T=0 K zero for sample #146. Carbon could be a good candidate although it remains at the level of a hypothesis, since the background carbon contamination is hard to detect. However, as already mentioned, carbon contamination is to be expected in MOVPE processes, especially when graphite heater is used, as in our experimental set-up.

Looking for other defects in bulk β-Ga_2O, with energy states positioned at about 0.7 eV below CB, we have to recall the levels at 0.6 eV (E1), 0.8 eV (E2 and E2*) and 1 eV (E3) detected by space charge spectroscopy. However, they have been identified as *electron traps* [48,49,50,51], not as donors, and their microscopic origin is not yet known; some of them being attributed to unintentional ubiquitous contaminants such as Fe [52], or to complexes of native defects and hydrogen [50,53]. Hydrogen contamination seems indeed to play a crucial role in Ga_2O_3. In Ref. [33], hydrogen-V_{Ga} complexes were predicted to behave as compensating acceptors with lower formation energy than the isolated vacancies. However, the formation of complexes of hydrogen with native defects in β phase is still a matter of debate [54]. Furthermore, hydrogen has been

predicted to introduce also *shallow* donors in β-Ga$_2$O$_3$ [44], although contradictory interpretations have been reported [53]. In β-Ga$_2$O$_3$, interstitial hydrogen is expected to act as an electrically active defect [33,55-57]; experimental support for the shallow donor nature of hydrogen comes from the weak binding energy measured for muons in β-Ga$_2$O$_3$ [58]. Ref. [59] provided a review of hole and electron traps in as-grown and irradiated β-Ga$_2$O$_3$.

In MOVPE, the use of H$_2$O as an oxygen source surely makes a great amount of hydrogen available in the reactor, even greater when H$_2$ is used as a carrier gas, therefore, hydrogen incorporation is likely to occur also in our ε-Ga$_2$O$_3$. The presence of shallow donor states associated with hydrogen is suggested by the lower resistivity values measured in our UD film grown with H$_2$ carrier gas with respect to He (≈10^7 Ωcm against 10^{13} Ωcm), as well as a lower thermal activation energy of the conductance. Less probable, and more speculative, is the alternative hypothesis of He-induced compensation to justify the higher resistivity of He-carrier samples. Certainly, the presence of deep acceptors in UD films, grown with either H$_2$ or He carrier, is responsible for the compensation of hydrogen-related shallow donors, providing different resistivity values depending on the relative density of incorporated hydrogen and/or on other defects related to the carrier gas.

Furthermore, the resistivity behavior with temperature of the highly resistive ε-Ga$_2$O$_3$ also requires the action of acceptors, whose presence was confirmed by recent CL measurements [31].

In conclusion, it is reasonable to assume that hydrogen-related shallow donors, carbon and oxygen-vacancy deep donors as well as deep acceptors determine the measured Fermi energy and thus the temperature dependence of the electrical conductivity in nominally undoped ε-Ga$_2$O$_3$. Full compensation of hydrogen shallow donors by acceptors leads to high resistivity, whose temperature dependence is mainly related to the occupancy variation of C and V$_O$ deep donors.

1. 2 Thermally and Photo-induced persistent conductivity effects

Persistent Photo-Conductivity (PPC) and Persistent Thermally-induced Increase of Resistivity (PTIR) have been observed in ε-Ga_2O_3. These phenomena can be related to charge state variation of either intrinsic defects or impurities having non-equilibrium occupancy. The PPC effect occurs when deep levels possess an energy barrier higher than thermal energy against re-capture of photo-generated carriers. To explain PTIR, we have to assume the presence of defects exhibiting an energy barrier for the thermal capture of carriers, generally associated with a local lattice distortion. The increase in temperature well above RT can provide more and more thermal energy to carriers, so they overcome the energy barrier, but remain trapped while going down to RT temperature. The distortion could also induce a negative value of the Hubbard energy forming a negative-U center [61].

Various defects in β-Ga_2O_3 have been predicted to behave as negative-U centers: among them C impurity [34], and the oxygen vacancy V_O [44], as mentioned above. In a recent EPR study [60], the Si shallow donor in β-Ga_2O_3 has been claimed to behave *DX*-like. Instead, Neal et al. [51] and Lany [34] excluded a negative-U behavior for Si donor in β-Ga_2O_3. On the other hand, Lyons predicted a negative-U behavior for V_O defect *for all* Ga_2O_3 phases [37].

We observed significant PTIR effect in several ε-Ga_2O_3 samples grown with carrier H_2, both undoped or doped. PPC effects, instead, were mainly observed at low-temperature in some Si-doped films, where generally PTIR was not detected. A systematic investigation of these puzzling and irreproducible phenomena, probably unrelated to each other, was not yet performed.

In doped layers, PPC was observed by exciting the sample with a white light source during the cooling down to 10 K, and then switching off the light source during the subsequent heating up to

RT. Persistency of the photoconductivity was observed at least up to RT. Red light did not induce PPC. Both observations suggest that the deep centers giving PPC are characterized by high energy barriers affecting both thermal-capture and optical-emission of electrons.

In unintentionally doped high resistivity samples, the response to light is significant only for photon energy above the bandgap, which generally induces high RT-photoconductive response (see paragraph 1.3 and Fig. 5). Long times are requested for relaxation after on/off light cycles: at low temperatures, the off-response times become extremely long, and the photocurrent almost persistent. In some undoped samples, an irreversible increase of the dark current was observed after exposure to bandgap radiation, without canceling the photoconductive response. All phenomena are certainly related to the presence of deep levels.

The PTIR effect appeared as a dual behavior of the resistivity during a cycle of heating above RT and subsequent cooling to RT, with higher resistivity values during the second step of this cycle. The variation of the RT resistivity was persistent in time and dependent on the highest temperature and duration of the measurement: a change in resistivity of one order of magnitude was observed after the sample was heated up to 600 K for a few hours, and then was cooled back to RT. However, the heating ramp and the maximum temperature reached in these cycles were seen to modify the results. The resistance increase persisted even after months, and the initial conductivity could not be optically restored. The PTIR phenomenology could also be explained by an irreversible escape of hydrogen during the sample heating. In fact, the loss of hydrogen (known to be a shallow donor) could justify the conductivity reduction. Unfortunately, so far we have not a direct evidence of hydrogen outdiffusion. It could also be that both phenomena, non-equilibrium occupancy of deep levels and hydrogen escape, simultaneously contribute to PTIR.

For completeness, we mention that also surface states could contribute to PPC and PTIR, eventually influencing the surface band bending. It is worth recalling that effects of surface depletion due to hydrogen incorporation from the external environment have been pointed out for the β-phase [53,62], and cannot be ruled out in ε-Ga$_2$O$_3$.

1.3 Native deep acceptors in UD ε-Ga$_2$O$_3$

Acceptor states in ε-Ga$_2$O$_3$ are expected to be deep, due to the very flat VB states revealed by ARPES [25]; self-trapping of holes has been predicted, as in the β-phase [37]. Oxygen interstitials and Ga vacancies can form easily due to the complicated 4H-stacking sequence of the ε-Ga$_2$O$_3$ structure [10] and are good candidates to be intrinsic acceptors. However, the formation of stable O-interstitials seems less probable owing to the tendency of oxygen to escape from the compound.

Among the extrinsic acceptors, Mg has been predicted to introduce a deep acceptor level in ε-Ga$_2$O$_3$ [37]. According to recent CL investigations [31], nitrogen can be equally suspected to introduce a deep acceptor, as reported for β-Ga$_2$O$_3$ [39,63]. However, in the β phase it was also reported that it can also behave as a deep donor when in interstitial site or forming complexes ((N_2)$_{Ga}$ and (N_2)$_O$ [64]).

Experimental evidence of a band of deep acceptor states above the VB maximum in our ε-Ga$_2$O$_3$ has been provided by ARPES. These levels are expected to be related to bulk lattice defects, as surface states are supposed to play a negligible role owing to the absence of significant surface band bending in the investigated sample [25].

A confirmation of the existence of deep acceptors has been given in Ref. [31] by a CL broad band emission composed by four Gaussian peaks centered at 2.4 eV (517 nm), 2.75 eV (450 nm), 3.0 eV (413 nm), and 3.15 eV (394 nm). The relative intensities of the peaks depend on the growth

conditions, whereas the energy positions are practically independent of growth parameters and carrier gas [31]. A tendency to decrease the intensity of the CL emission with temperature was generally observed, although the thermal quenching of the CL intensity resulted sample dependent.

We report here new CL investigations performed on a highly resistive film (#146) with a thickness of about 500 nm. The CL was excited with an electron beam energy of 20 KeV, for which the expected probe depth was ≈ 0.7 μm and excitation involves both substrate and epilayer. At lower beam energy CL spectra are very noisy and affected by surface contributions. To discriminate the Al_2O_3 emissions, CL spectra of a bare sapphire substrate were recorded in the same experimental conditions. Figs.4a and 4b show the CL emission of sample #146 (black thick curves) measured at T=80 K and T=300 K, compared to the corresponding spectra of the Al_2O_3 substrate (red thin curves). At 80 K one observes the broad band between 2 eV and 3.4 eV, and an additional band around 1.67 eV, which partly overlaps the bands from the sapphire substrate. A similar emission has been recently reported by Shapenkov et al. [32].

The temperature dependence of the broad CL band is plotted in Fig.4c, in the range (2.2-3.3) eV to exclude the 3.7 eV substrate peak. These spectra are compatible with the deep energy states mentioned above (see also Ref. [31], in particular the sample #479 grown with He-carrier gas), and can be deconvoluted into the same Gaussian peaks, but with different relative intensity: a monotonic decrease of the CL intensity with temperature is clearly visible. A quantitative fit of these data, however, is considered not reliable due to the unavoidable contribution of the substrate emission. The present results confirm previous CL emission spectrum and its temperature dependence. In Fig.4b one can appreciate that at RT the broad band (2.0-3.4) eV is very weak, while the thermal quenching is not so effective for the 1.67 eV peak. The small influence of the growth conditions [31] on the energy positions of the four CL peaks, in contrast to intensity

variations, and the similarities of spectra reported by several authors (Refs. [31], [32] and

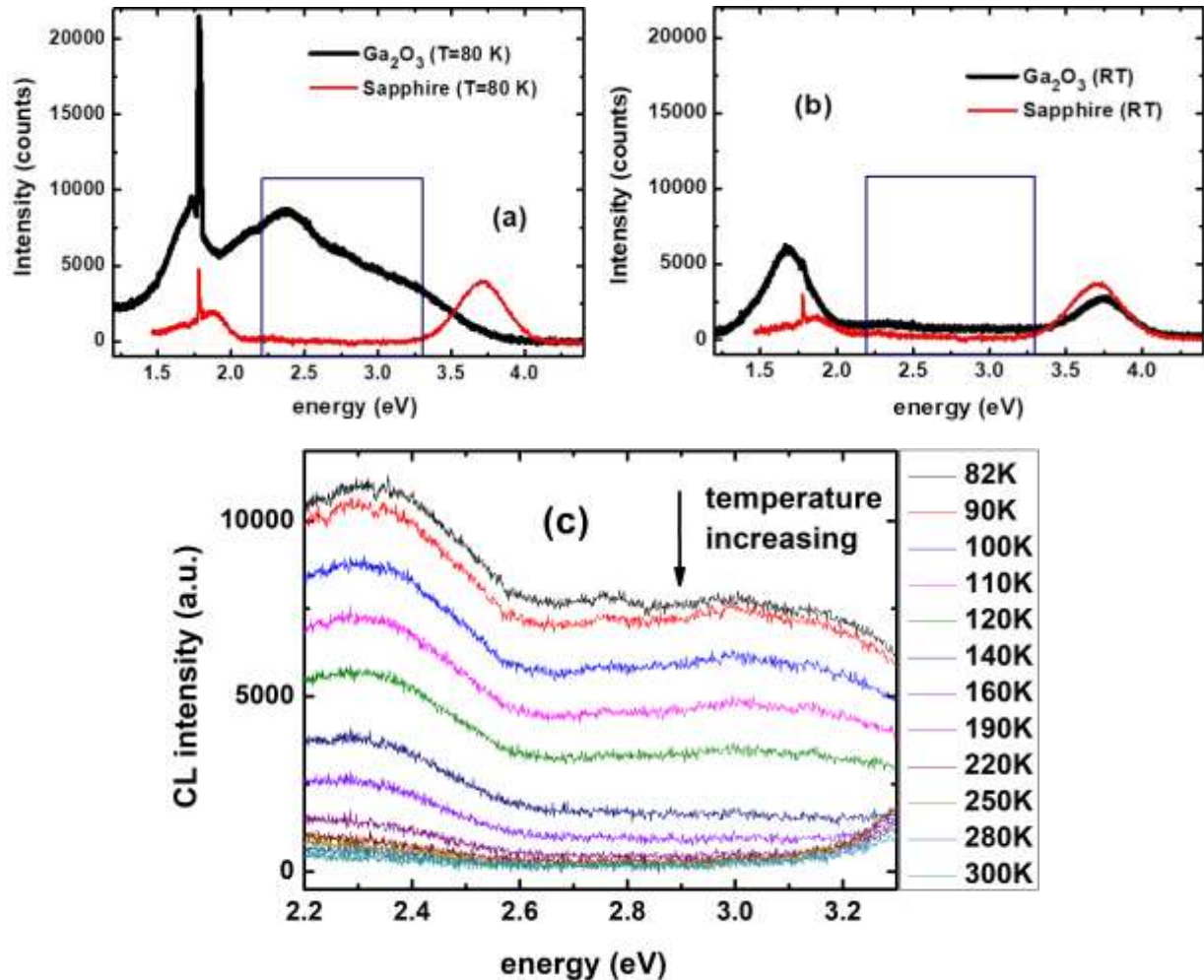Supporting Information of Ref. [42]), suggests the involvement of intrinsic lattice defects, rather

Fig.4 (a,b) Black thick curve: CL of #146 sample; red thin curve: CL of the Al_2O_3 substrate at (a)

T=80 K (b) RT on a wide energy range. The frames in (a) and (b) are added to evidence the spectral

region of (c). (c) CL spectrum of #146 sample at different temperatures in the spectral range where

the CL emission from the substrate is negligible. The energy of the exciting electron beam was 20

KeV for all spectra. No baseline subtraction has been performed in the spectra. At the highest

temperatures the increase of the intensity at about 3.2 eV is due to the non-negligible emission of the

substrate.

than of contaminants connected with the growth process.

Interestingly, the broad CL spectrum shown in Fig.4c monotonically decreases with increasing temperature for sample #146, whereas in the thick UD sample discussed in Ref. [31] (named #425) a maximum of the CL intensity was observed at about 100 K. In Ref. [31], this feature was attributed to thermal activation of electrons from shallow donor states to the CB states prior to its radiative decay. To understand the reason for the different behavior with T let us consider the differences between the two samples: (i) the carrier gas was He for sample #146 and H_2 for the UD sample of Ref. [31]; (ii) the RT dark resistivity was $\approx 10^{13}$ Ωcm for sample #146 and 10^4 Ωcm for #425, a value lower that the usual one for nominally UD material, which suggests a significant shallow donor contamination; (iii) the layer thickness, 0.5 μm for #146 vs 6 μm for #425. Considering point (i), one can argue that hydrogen might contribute to this phenomenology. However, one cannot neglect the presence of a surface potential that could empty the shallower traps, making the thin layer significantly depleted.

To gather further information on the electronic states in sample #146, spectral photoresponse was performed and the corresponding calibrated results are reported in Fig.5a. There is a negligible photoresponse below 4.4 eV, which suggests that the very high resistivity of this sample might be related to an extremely low density of shallow donors, coupled to a low density of in-gap states. For comparison, the inset of the Fig.5a shows the responsivity curve of another UD ε-Ga_2O_3 layer, showing a remarkable photoresponse in the sub-bandgap visible-near UV range. It clearly appears that a relatively high density of deep states coincides with a lower ratio between intensity of UV and visible radiations (UV-visible rejection ratio). This ratio is indicative of the solar-blind behavior of a detector. Note that the ratio is instead 10^4 for sample #146; this is probably the

highest responsivity ever reported for ε-Ga$_2$O$_3$, which is a qualifying feature for UV-C detection applications.
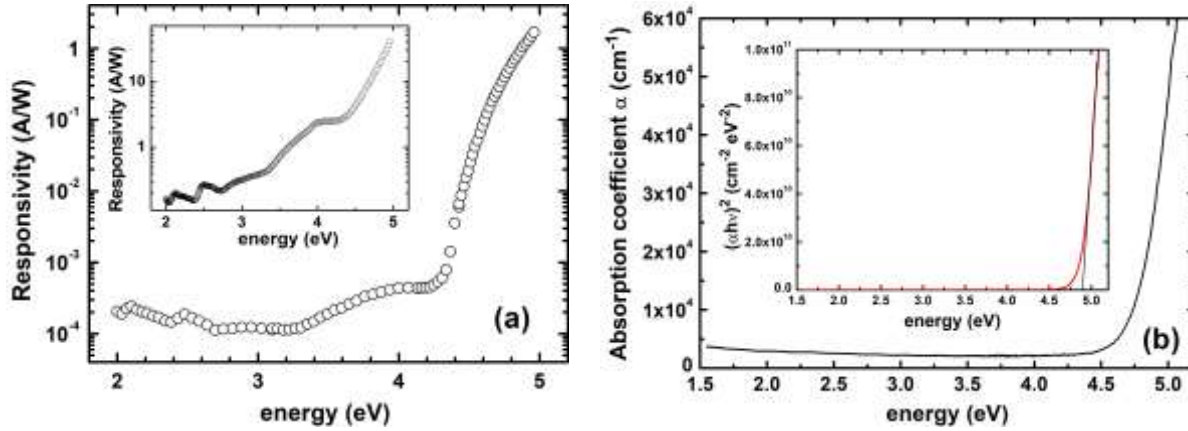

Fig.5 (a) RT Spectral responsivity for the sample #146. Insert: responsivity of a sample showing a significant density of in-gap states. (b) RT Optical absorption spectrum for the sample #146 in proximity of the optical edge and Tauc plot of the same data in the insert.

Concerning the OAM below the band edge for the sample #146, the signal is almost negligible up to (4.6-4.7) eV; the corresponding absorption coefficient is shown in Fig.5b. It evidences a sharp increase at 4.6-4.7 eV, whereas a standard Tauc plot (inset of Fig.5b), conventionally used to extrapolate the bandgap value, indicates a bandgap of about 4.9 eV, consistent with the result of Ref. [13]. However, as discussed in Ref. [30], the analysis of experimental absorbance data through a Tauc plot leads to an extrapolated absorption edge dependent on the layer thickness, which has no physical meaning. For this reason, we consider the onset in the linear plot of both the absorption coefficient spectrum and photocurrent spectrum as a lower estimate of the bandgap of #146 sample. Then, the value of 4.7 eV has been used in the summary scheme of Fig.6.

It is reasonable to suppose that the same set of deep defects participate in both PC and CL processes. In principle, both deep donor and acceptor states could be involved; however, acceptor

defects seem more probable considering the results of the ARPES study. In particular, V_{Ga} acceptors or their complexes could play a main role, as was also suggested for β-Ga$_2$O$_3$ in [65].

To account for the results of optical, electrical and photoelectrical investigations on UD samples, we propose the scheme of Fig.6. It can consistently explain: (i) the four CL emission bands in the
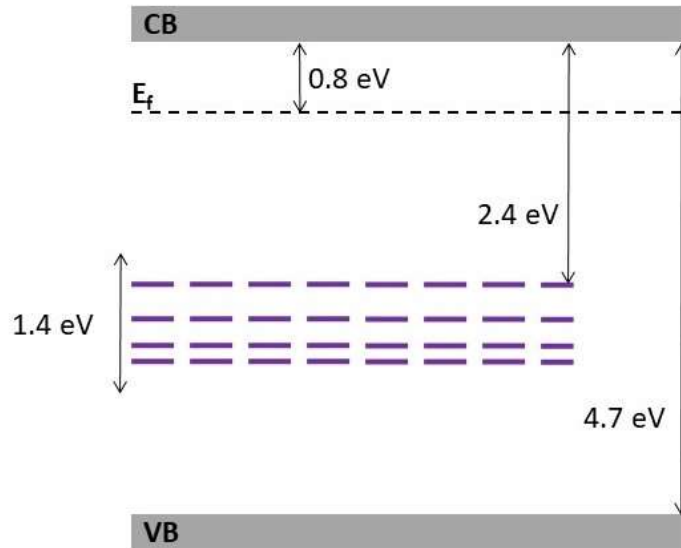

Fig.6 Schematic deep level structure for ε-Ga$_2$O$_3$ films, consistent with both CL and PC results. Shallow and deep donor levels are not reported because they are not supposed to be involved in the radiative transitions. The equilibrium Fermi level is placed at (E$_c$-0.8) eV, as determined for sample #146.

broad energy range 2.0-3.4 eV, interpreted as radiative transitions from the CB to acceptor levels; (ii) the agreement between CL and PC; (iii) the previous ARPES measurements, which indicate the presence of a broad band related to deep acceptors [25]. The equilibrium Fermi level is located at (E$_c$-0.8) eV, as determined for sample #146.

2. Silicon-doped ε-Ga$_2$O$_3$ layers

Low-resistivity n-type ε-Ga$_2$O$_3$ layers were obtained by in-situ doping with Si, during MOVPE growth with H$_2$ carrier. Si substituting Ga on the tetrahedral sites in ε-Ga$_2$O$_3$ is a shallow donor, as evidenced by EPR spectroscopy [27]. Indeed, only a single EPR peak was observed, excluding an appreciable incorporation of Si on the other three non-equivalent octahedral lattice sites. Moreover, a nearly constant g-value close to 1.95 was observed in the (4-300) K temperature range, as expected for a neutral effective-mass-like donor or free electrons. A uniform distribution of Si has been demonstrated by Time of Flight-Secondary Ion Mass Spectrometry analysis [38].

The n-type conductivity induced by Si-doping was confirmed by a negative Hall coefficient, RT electron densities in the range $(10^{17}$-$10^{18})$ cm^{-3}, and low mobility values of a few cm^2/Vs [38]. The conductivity shows two linear regions, with different slopes, when its natural logarithm is plotted vs. T$^{-1/4}$ (*Mott plot*). This indicates a variable range hopping conduction, described by the Mott law: $\sigma(T) \propto \exp\left[-(T_0/T)^{1/4}\right]$, where $T_0 = C/(\xi^3 g(\mu) k_B)$ [66,67] is a reference temperature depending on the density of states $g(\mu)$ at the μ Fermi level; k_B is the Boltzmann constant; $g(\mu)$ is assumed to be constant, i.e. electron-electron interaction is neglected [66,67]. T_0 depends on the localization radius ξ, which characterizes the spatial extension of the wave-function. The proportionality constant C is a dimensionless parameter dependent on the network of hopping sites. A hopping transport mechanism is generally observed at low temperature in doped samples, with a shift of the onset toward higher temperature by increasing the doping level. The variable-range-hopping (VRH) transport prevails on the mechanism of thermally activated nearest-neighbor-hopping (NNH) at low enough temperature. However, structural disorder contributes to localization of carriers on defects, reducing the coherence length of the carrier wavefunction, and in doped material it favors the impurity band conduction with a transport by VRH. In disordered systems the VRH conduction can prevail at any temperature [66,67].

The transport by VRH shown in Ref. [38] is supposed to take place between the localized states of the Si-donors. In Ref. [27] the two-slope behavior has been explained by assuming that at the lower temperatures hopping conduction occurs through the states of isolated Si-donors (LT-VRH). Differently, at higher temperatures the transport is done by hopping (HT-VRH) between Si-donor clusters, i.e. states which lie near the CB bottom, resulting from the hybridization of quasi-atomic and extended states; they are characterized by a greater delocalization of the Si-electron wavefunction [27,68]. Such two-slope linear behavior of the *Mott plot* is not just peculiar of Si-doping because it was also observed in *n*-type ε-Ga$_2$O$_3$ doped with Sn introduced by diffusion [38,69]. This impurity is incorporated and behaves as a donor [69,70], although often also used as a surfactant in physical deposition methods [20,71,72]. This suggests that the peculiar defect structure (rotation domains) of ε-Ga$_2$O$_3$ might be at the origin of the observed VRH.

The *Mott plot* for two Si-doped samples exhibiting the highest conductivity obtained up to now is shown in Fig.7a. The samples were neither illuminated nor heated. The previously cited two-slope linear trend is clearly observed and the corresponding slopes are reported in Table 2, along with the conductivity and the Hall carrier density of both samples, to underline the self-consistency of the data. Indeed, the slopes in linear *Mott plots* are inversely proportional to $g(\mu)$ and so, ultimately, to the volume density of the hopping sites, i.e. the Si density for LT-VRH. Therefore, the lower the slope, the higher the doping level and the Hall density. Such a consistency between conductivity values, and the slopes of the linear traits of the *Mott plots,* and measured RT Hall density for several samples of different thickness [38] is a result supporting a bulk transport rather than surface transport.

By evaluating the density of the localized defects involved in the VRH conduction from the *Mott plot* slopes, we obtained values of the order of 10^{19} cm^{-3} for both the #440 and #335 samples. These

densities become comparable with the RT carrier concentrations measured by Hall effect only if we assume a significant electrical compensation. Such a high compensation may be explained by a significant density of V_{Ga} (and related complexes) and/or residual C impurities in a negative charge state. Comparable RT spin density is obtained by EPR for the two samples, equal to 2.1×10^{18} cm^{-3}, consistent with the Hall density [27].

Table 2. *Mott plot* slopes and Hall density for the samples #335 and #440

	Sample #335	Sample #440
Slope LT-VRH [K$^{1/4}$]	-5.2 ± 0.2	-3.7 ± 0.2
Slope HT-VRH [K$^{1/4}$]	-10.8 ± 0.1	-9.9 ± 0.1
Hall density [cm^{-3}]	2.9×10^{18}	3.7×10^{18}
RT conductivity [Ω^{-1} cm^{-1}]	2.13	2.38

Hall carrier density and mobility for the more conductive #440 sample in the temperature range 40 – 600 K are shown in Figs.7b and 7c. This is the widest temperature range for transport investigation of this polymorph, and provides a convincing support to the VRH transport mechanism in the whole temperature range. A comparison with transport data obtained in β-Ga$_2$O$_3$ with similar doping level, shows a different behavior: in β-Ga$_2$O$_3$, electron freezing and a Hall mobility maximum at about 100K, with typical absolute values always higher than 100 cm^2/Vs, guarantee the occurrence of a transport into the CB extended states [49,73,74]. Hall data of ε-Ga$_2$O$_3$ show instead a nearly temperature-independent Hall density, with negligible freezing, and a monotonic increase of mobility with temperature, consistent with higher hopping probability. These features support the hypothesis of a VRH transport mechanism at any temperature in the
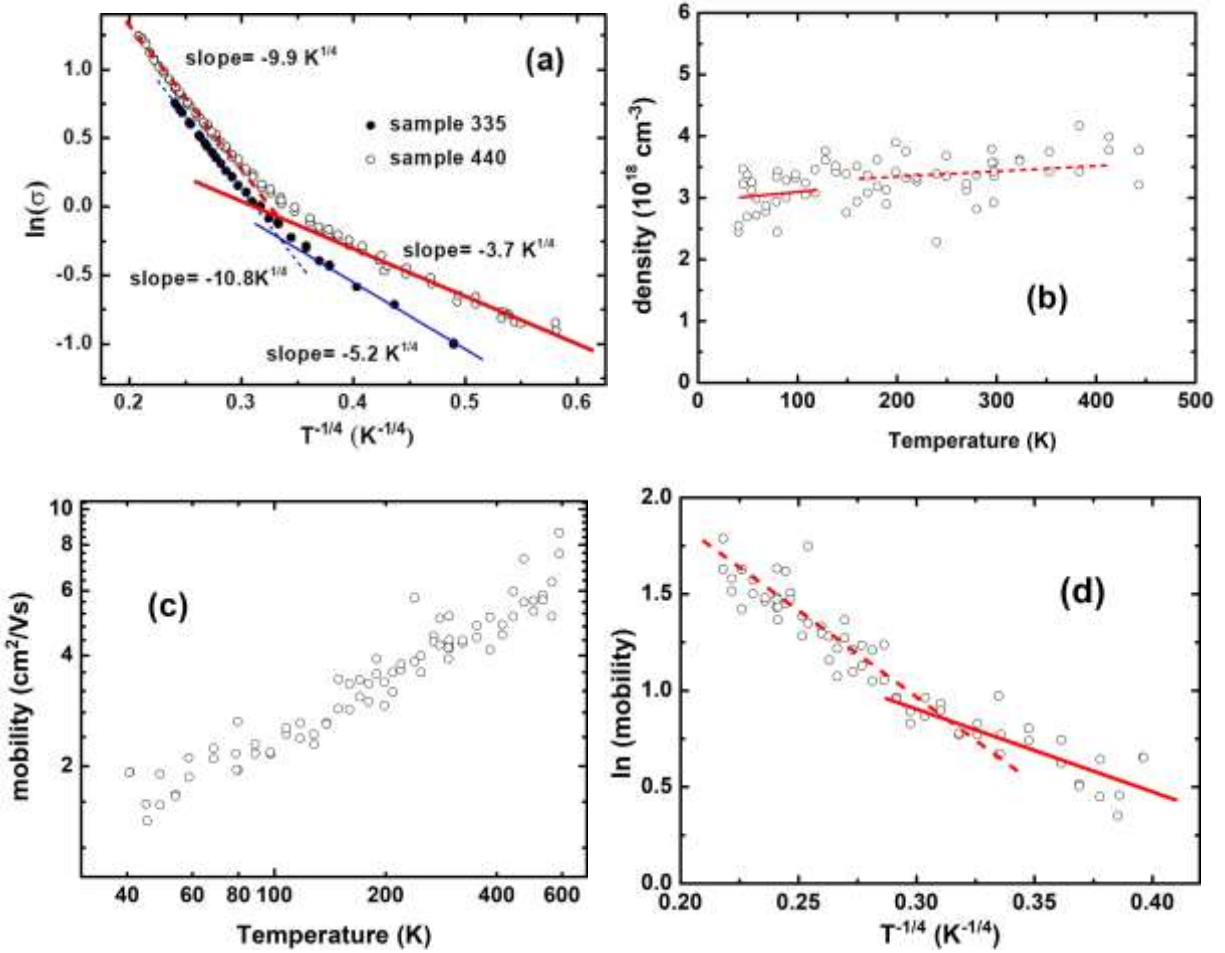
Fig.7 (a) *Mott plot* of the conductivity (in Ω^{-1} cm^{-1}) in the Si-doped samples #335 (full circle) and #440 (empty circle). Continuous lines: LT-VRH trends; dashed lines: HT-VRH trends in both samples, in red (thick) for sample #440 and in blue (thin) for sample #335. More heavily doped sample, #440: (b) temperature dependence of Hall electron density; (c) Hall mobility vs. T in log-log scale. (d) *Mott plot* of the mobility data (in cm^2/V·s) for sample #440. Lines are a qualitative guide for the eye.

whole investigated temperature range. Moreover, it is reasonable to argue that the two different LT-VRH and HT-VRH transport regimes could appear also in the carrier density and mobility plots. Indeed, in the *Mott plot* of Fig.7d it is possible to recognize two slopes, despite the experimental data scattering.

It is interesting to note that such linear trend of the *Mott plot* again appears after illuminating the sample at low temperature when the PPC effect is observed, suggesting that this phenomenon is due to higher density of carriers photo-excited from traps and moving through localized states. Such a phenomenology was detected only in a few Si- or Sn-doped samples with carrier density of about 10^{17} cm^{-3}, while in the most conductive samples PTIR was generally observed. Fig.8a shows the *Mott plot* of the conductivity measured in a lightly Si-doped sample (#307: see table I), under different conditions, as detailed in the caption. After each step the RT conductivity was tested, and the same value was found. The heating of this sample did not induce any PTIR effect.

On the other hand, in more conductive samples, PTIR effect was observed after heating a sample above RT, but no PPC phenomena appeared (Fig. 8b). The phenomenon is independent of the electrical-contact stacks, that are different in samples #335 and #440 (see Experimental Section), suggesting a negligible effect of Au diffusion if any. A linear trend of the conductivity data in the *Mott plot* is again observed, in agreement with the hypothesis of a variation (in this case a reduction) of the carrier density involved in the VRH conduction, hence confirming the transport model.

The EPR plot of sample #440 is given in Fig.9 and compared with previous published data for sample #335 [27]. The spectra are in very good agreement in terms of temperature dependence of the EPR linewidth and signal intensity. Comparable spin density at RT was measured in the two samples, in good agreement with the RT Hall densities. The EPR spectra of the Si donor showed, depending on temperature, Gaussian and Lorentzian line shapes as expected for delocalized electrons or carriers localized on donors. The linewidth of the shallow donor resonance varies strongly with temperature, and its analysis gives insight into the carrier dynamics. Three regimes of transport are identified, i.e. fully localized electron, hopping transport - more precisely VRH

transport - and fully delocalized electrons. The *Mott plot* of the EPR linewidth reported in Fig.9b evidences slightly smaller values in the #440 sample with respect to #335 in the temperature range of the VRH transport (these samples were neither heated nor illuminated), indicative of a higher
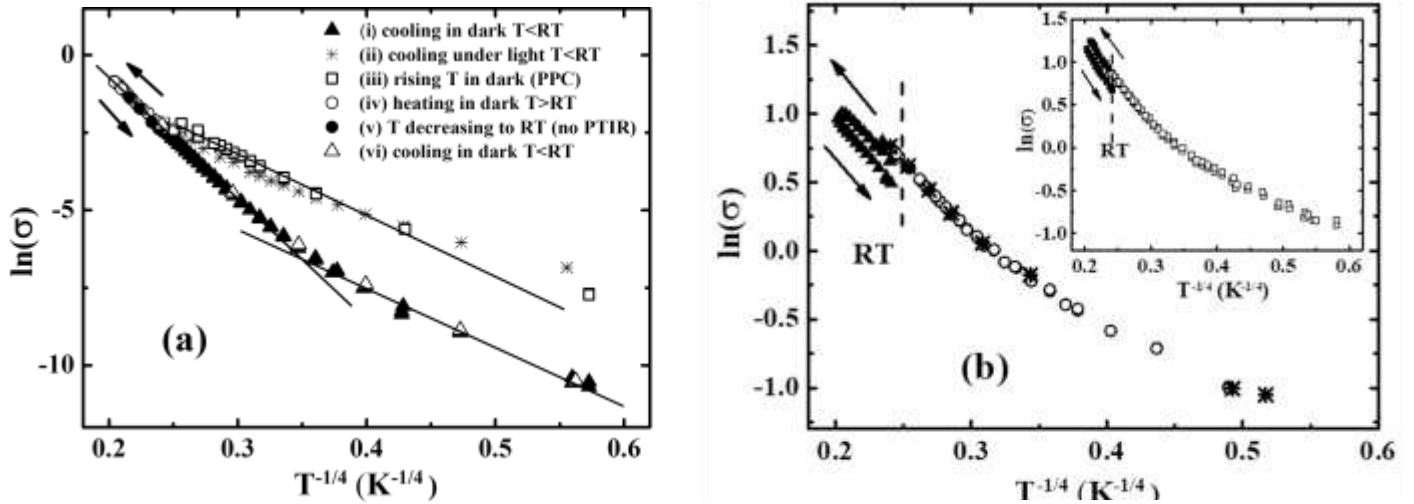

Fig. 8 (a) Sample #307, Si-doped, $n \approx 10^{17}$ cm^{-3} [38]: *Mott plot* of the conductivity evidencing the PPC effect, whereas PTIR effect is not observed. The data were taken following this sequence: (i) cooling in dark (full triangles); (ii) cooling under white light (asterisks) and (iii) rising to RT in dark after turning off the light (open squares), showing PPC; (iv) heating above RT in dark (full circles); (v) temperature reduction to RT, without PTIR; (vi) cooling again to low T (open triangles), as reproducibility test. (b) Sample #335: *Mott plot* of the conductivity evidencing PTIR effect, whereas PPC effect is not observed. The data were taken following this sequence: (i) cooling in dark (empty circles); (ii) cooling under white light and turning off the light at the lowest temperature (asterisks): no evidence of PPC; (iii) reduction of the RT conductivity after short heating of the sample at about 450 K (not shown); (iv) heating up to 600 K and subsequent decreasing to RT in dark (full triangles): the data taken returning to RT are shifted to lower values (PTIR): the shift depends on the residence time at the highest T. Insert: steps (i) and (iv) for sample #440. In all the figures, arrows near the data help to distinguish data taken for increasing and decreasing temperature.

conductivity, in agreement with the transport measurements. In fact, a smaller linewidth indicates a more effective motional narrowing, as well as a higher hopping frequency and probability.

The conductivity and EPR data of Fig.7a and 9b are similar in a wide temperature range, showing little differences in the absolute value of the *Mott plot* slopes. However, close to RT, EPR indicates spin resonance by delocalized electrons for both samples, whereas the electrical conductivity data still show VRH transport, even above RT up to 600K. This apparent contradiction was resolved in Ref. [27] by assuming the formation of shallow donor clusters, wherein electrons can freely move; their spins appear then delocalized to EPR, which mainly reflects the localization length of the electron wavefunction at a local scale (short range order) [68]. However, donor clusters are
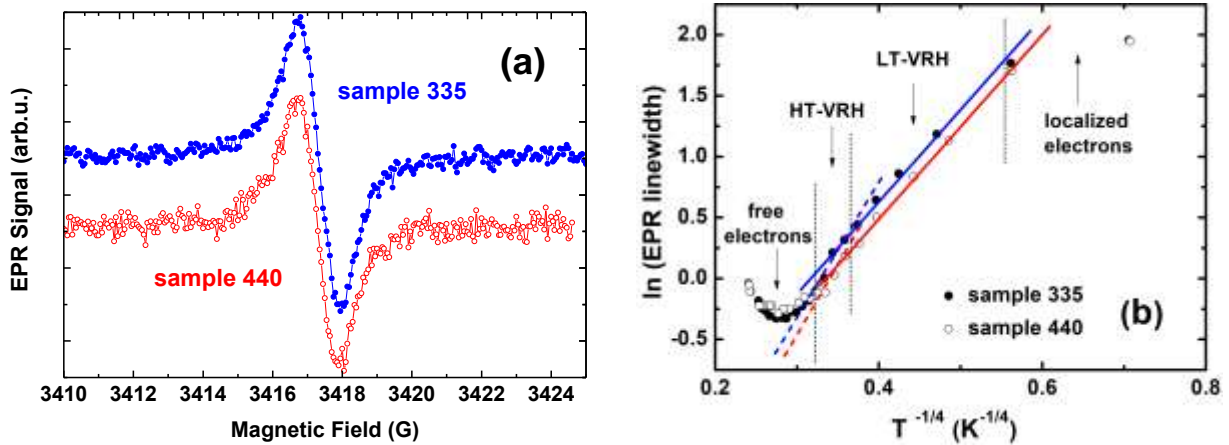

Fig.9 (a) RT Si donor related EPR spectra (B-field parallel to the c-axis) and (b) the T-dependence of the EPR linewidth for samples #335 and #440.

spatially separated, so that the dc conductivity again indicates electron transport via hopping. Structural disorder, related to the presence of 120° rotational domains, is likely involved in this localization effect.

Si incorporation on tetrahedral Ga sites as hydrogenic donor, in analogy to the case of β-Ga₂O₃, is a most interesting result of EPR study. The RT spin density found in ε-Ga$_2$O$_3$ is comparable to

that reported for both α- and β-phases, which corroborates the value of about 36 meV for the electron binding energy of the Si-donor estimated for other polymorphs. This implies a value of about 0.3 m_e for the electron effective mass of ε-Ga$_2$O$_3$, very comparable to previous estimates for other Ga$_2$O$_3$ phases. It should be noted that this is the first estimate of the CB effective mass for ε-Ga$_2$O$_3$. In addition, as in ε-Ga$_2$O$_3$ the g-tensor anisotropy is small (Δg=0.0018), the effective mass anisotropy is also expected to be weak [27].

3. Shallow donors - deep defects interaction

It has recently been demonstrated that Si-doping drastically reduces the CL emission and also modifies the relative intensity of the four-Gaussian peaks obtained by deconvolution of the CL broad band ranging from 2 eV to 3.4 eV [31]. There are two ways to explain the CL drop: first, one can consider that Si, in addition to forming shallow levels, may also give rise to non-radiative complex defects or, second, Si can suppress the formation of the deep acceptor centers located at (2.4-3.15) eV from CB. It becomes thus important to examine the possible interactions between shallow and deep defects in ε-Ga$_2$O$_3$.

As Si on tetrahedral Ga behaves as a shallow donor, the formation of V_{Ga}-related deep acceptors is in competition with the occupancy of Ga sites by Si. An example of such defects is the split-vacancy complex, whose formation has been theoretically predicted [33,34] and experimentally observed in irradiated β-Ga$_2$O$_3$ [35,36]; it corresponds to two tetrahedral V_{Ga} with an interstitial Ga in between. Another V_{Ga}-related defect detected by EPR in β-Ga$_2$O$_3$ is the octahedral gallium mono-vacancy. The formation of V_{Ga}-H complexes has also been predicted [33]. Considering our present results and the literature data, we suggest that a high density of Si, occupying Ga-sites, can reduce the density of one (or more) type of V_{Ga}-related centers. This in turn reduces the

concentration of deep acceptors and the related radiative transitions. This hypothesis however partially clashes with ref. [75], where Si doping in β-Ga_2O_3 was indicated to increase the concentration of Ga-vacancies due to self-compensation, a known phenomenon that has been predicted to represent a serious limitation to the maximum obtainable free carrier concentration in Ga_2O_3 compounds [34].

On the other hand, shallow donors can be complexed (and passivated) by other point defects to give rise to non-radiative recombination levels. A complex "split Ga vacancy structure - dopant atom in interstitial site" was actually proposed for β-Ga_2O_3 [34]. To further complicate the scene, the growth environment, H_2, He or N_2, can also play a role in the formation of complexes (e.g. V_{Ga}-H complexes). When silane is used for doping and N_2 as carrier gas, the CL quenching is even more pronounced. This result can reasonably be explained by considering that nitrogen itself acts as a deep acceptor, not contributing to CL transitions, but rather altering the density of deep acceptors related to Ga-vacancy, in detriment of the radiative transitions. Furthermore, for the same flux of silane, films grown with N_2 carrier gas are much more resistive than films grown using H_2 carrier, which indicates a heavier compensation, supporting the idea of nitrogen as an acceptor level in ϵ-Ga_2O_3. Another convincing experimental evidence for nitrogen acting as deep acceptor is given by a series of Sn-diffusion experiments in ϵ-Ga_2O_3 films [38,69]: high-resistivity as-grown epilayers, obtained with H_2 or He carrier gases, readily converted to semiconducting upon Sn diffusion, with resistivity of few Ωcm, while epilayers deposited with N_2 carrier gas, submitted to the same diffusion process, remained highly resistive. Nitrogen was indeed reported to be a deep acceptor in β-Ga_2O_3 [39,63], but so far there were no literature data on the actual role of nitrogen in other polymorphs, therefore, our present observations represent the first direct indication of nitrogen as compensating impurity in ϵ-Ga_2O_3.

Conclusions

CL and PC spectroscopy, optical absorption, temperature dependent resistivity and EPR measurements on doped and undoped ε-Ga$_2$O$_3$ epilayers, grown by MOVPE under different carrier gases, were presented in this work. Temperature-dependent resistivity and optical investigations were performed on the same highly resistive sample permitting a reliable correlation of the results. Transport data were measured for the first time in a wide temperature range on Si doped films, giving strong support to the interpretation of the transport mechanism as due to VRH. Additional EPR data were shown, reinforcing the experimental frame and the conclusions on the conduction band features.

This comprehensive characterization provided new insights into origin and properties of deep and shallow levels in ε-Ga$_2$O$_3$ which can be summarized as follows:

Formation of deep levels may be ascribed to Ga vacancies and/or their complexes (acceptors), oxygen vacancies (donors) as well as to impurities, such as carbon (donor) and nitrogen (acceptor). The Fermi level position in the most resistive (He carrier) UD layers was seen to be positioned at about 0.8 eV below the CB minimum, which provides a resistivity of about 10^{13} Ωcm, extrapolated at RT; the balance between carbon donors and compensating acceptors, is believed to be responsible of the deep Fermi energy and high resistivity of nominally-undoped samples. The use of H$_2$ as carrier gas provided samples with consistently lower resistivity, which points at hydrogen as shallow donor in ε-Ga$_2$O$_3$.

A model for the CL emission and extrinsic PC spectroscopy based on transitions between CB and deep acceptor states was presented. This idea is well supported by previous ARPES

investigations that demonstrated the presence of a deep acceptor level in epitaxial ε-Ga$_2$O$_3$. The effects of in-gap states on the photoelectrical response of the material and possible non-equilibrium occupancy of deep energy states are here discussed for the first time.

The resistivity is below 1 Ωcm in Si-doped *n*-type samples, with a minimum RT value of 0.42 Ωcm, and an electron density of the order of 10^{18} cm^{-3}. The conduction through localized states (VRH) dominates the transport in *n*-type layers, evidenced here for the first time by Hall data in the 40 – 600 K temperature range. According to EPR, Si is an effective-mass donor, preferably substituting Ga on the tetrahedral site. Whilst EPR detected delocalized (free) electrons, it also confirmed the VRH transport mechanism.

A model that can reconcile the transport and EPR measurements consists of Si-related electrons contained within small volumes originated by donor clustering. Within such clusters the electrons are free to move, whereas the movement between clusters takes place by hopping. It remains still unclear if and how the domain structure of ε-Ga$_2$O$_3$ is involved in the observed electrical behaviour. A value of 0.3 m_e for the electron effective mass at Γ point, as well as little isotropy of the CB minimum, are confirmed by the present experiments.

Incorporation of process gases (hydrogen, helium or nitrogen carriers) plays a fundamental role in determining the physical properties of the epilayers, as they interact with intrinsic (lattice) point defects and may dramatically change the electrical and optical properties. UD samples grown under He have much higher resistivity than those grown with H$_2$-carrier. The use of N$_2$ as carrier gas, coupled to Si doping, may quench the CL emission; while He or H$_2$ carriers, with the same Si-doping, induce a much less pronounced CL intensity decrease. Intrinsic point defects and incorporated carrier gas species can also play a non-negligible role in the hopping conductivity, observed in Si-doped layers in the (10-600) K temperature range.

References

[1] Zhang, J.; J. Shi; Qi, D. C.; Chen, L.; Zhang, K. H. L. Recent progress on the electronic structure, defect, and doping properties of Ga_2O_3. *APL Mater.* **2020**, 8, 020906/1-35. https://doi.org/10.1063/1.5142999.

[2] Tsao, J. Y.; Chowdhury, S.; Hollis, M. A.; Jena, D.; Johnson, N. M.; Jones, K. A.; Kaplar, R. J.; Rajan, S.; Van de Walle, C. G.; Bellotti, E.; Chua, C. L.; Collazo, R.; Coltrin, M. E.; Cooper, J. A.; Evans, K. R.; Graham, S.; Grotjohn, T. A.; Heller, E. R.; Higashiwaki, M.; Islam, M. S.; Juodawlkis, P. W.; Khan, M. A.; Koehler, A. D.; Leach, J. H.; Mishra, U. K.; Nemanich, R. J.; Pilawa-Podgurski, R. C. N.; Shealy, J. B.; Sitar, Z.; Tadjer, M. J.; Witulski, A. F.; Wraback, M.; Simmons, J. A. Ultrawide-Bandgap Semiconductors: Research Opportunities and Challenges. *Adv. Electron. Mater.* **2018**, 4, 1600501/1-49. https://doi.org/10.1002/aelm.201600501.

[3] von Wenckstern, H. Group-III Sesquioxides: Growth; Physical Properties and Devices. *Adv. Electron. Mater*. **2017**, 3, 1600350/1-43. https://doi.org/10.1002/aelm.201600350.

[4] *Gallium Oxide: Materials Properties; Crystal Growth; and Devices* Springer Nature Editors: Higashiwaki, M.; Fujita, S. 2020. Springer Series in Materials Science.

[5] *Gallium Oxide- Technology: Technology; Devices and Applications* Edited by Pearton, S.; Ren, F.; Mastro, M. **2019**. Metal Oxides Series - Series Editor Ghenadii Korotcenkov.

[6] Pearton, S. J.; Yang, J.; Cary, P. H.; Ren, F.; Kim, J.; Tadjer, M. J.; Mastro, M. A. A review of Ga_2O_3 materials; processing; and devices. *Appl.Phys.Rev.* **2018**, 5, 011301/1-55. https://doi.org/10.1063/1.5006941.

[7] Galazka, Z. β-Ga_2O_3 for wide-bandgap electronics and optoelectronics. *Semicond. Sci. Technol.* **2018**, 33, 113001/1-61. https://doi.org/10.1088/1361-6641/aadf78.

[8] Playford, H. Y.; Hannon, A. C.; Barney, E. R.; Walton, R. I. Structures of Uncharacterised Polymorphs of Gallium Oxide from Total Neutron Diffraction. *Chem. Eur. J.* **2013**, 19, 2803-2813. https://doi.org/10.1002/chem.201203359.

[9] Fornari, R.; Pavesi, M.; Montedoro, V.; Klimm, D.; Mezzadri, F.; Cora, I.; Pécz, B.; Boschi, F.; Parisini, A.; Baraldi, A.; Ferrari, C.; Gombia, E.; Bosi, M. Thermal stability of ε-Ga_2O_3 polymorph. *Acta Mater*. **2017**, 140, 411-41. http://dx.doi.org/10.1016/j.actamat.2017.08.062.

[10] Cora, I.; Mezzadri, F.; Boschi, F.; Bosi, M.; Čaplovičová, M.; Calestani, G.; Dódony, I.; Pécz, B.; Fornari, R. The real structure of ε-Ga_2O_3 and its relation to the κ-phase. *CrystEngComm.* **2017**, 19, 1509-1516. https://doi.org/10.1039/c7ce00123a.

[11] Cho, S. B.; Mishra, R. Epitaxial engineering of polar ε-Ga_2O_3 for tunable two-dimensional electron gas at the heterointerface. *Appl Phys*. *Lett*. **2018**, 112, 162101/1-5. https://doi.org/10.1063/1.5019721.

[12] Mezzadri, F.; Calestani, G.; Boschi, F.; Delmonte, D.; Bosi, M.; Fornari, R. Crystal Structure and Ferroelectric Properties of ε-Ga_2O_3 Films Grown on (0001)-Sapphire. *Inorg Chem*. **2016**, 55, 12079–12084. https://doi.org/10.1021/acs.inorgchem.6b02244.

[13] Oshima, Y.; Víllora, E. G.; Matsushita, Y.; Yamamoto S.; Shimamura, K. Epitaxial growth of phase-pure ε-Ga_2O_3 by halide vapor phase epitaxy. *J. Appl. Phys*. **2015**, 118 085301/1-5. http://dx.doi.org/10.1063/1.4929417.

[14] Boschi, F.; Bosi, M.; Berzina, T.; Buffagni, E.; Ferrari, C.; Fornari, R. Hetero-epitaxy of ε-Ga_2O_3 layers by MOCVD and ALD. *J. Cryst. Growth* **2016**, 443, 25-30. http://dx.doi.org/10.1016/j.jcrysgro.2016.03.013

[15] Xia, X.; Chen, Y.; Feng, Q.; Liang, H.; Tao, P.; Xu, M.; Du, G. Hexagonal phase-pure wide band gap ε-Ga_2O_3 films grown on 6H-SiC substrates by metal organic chemical vapor deposition. *Appl. Phys. Lett*. **2016**, 108, 202103/1-5. http://dx.doi.org/10.1063/1.4950867.

[16] Yao, Y.; Okur, S.; Lyle, L. A. M.; Tompa, G. S.; Salagaj, T.; Sbrockey, N.; Davis, R. F.; Porter L. M. Growth and characterization of α-; β-; and ε-phases of Ga2O3 using MOCVD and HVPE techniques. *Mater. Res. Lett.* **2018**, 6, 268-275. https://doi.org/10.1080/21663831.2018.1443978.

[17] Nishinaka, H.; Tahara, D.; Yoshimoto, M. Heteroepitaxial growth of ε-Ga_2O_3 thin films on cubic (111) MgO and (111) yttria-stablized zirconia substrates by mist chemical vapor deposition. *Jpn J Appl Phys*. **2016**, 55, 1202BC/1-4. http://doi.org/10.7567/JJAP.55.1202BC.

[18] Tahara, D.; Nishinaka, H.; Morimoto, S.; Yoshimoto, M. Stoichiometric control for heteroepitaxial growth of smooth ε-Ga_2O_3 thin films on c-plane AlN templates by mist chemical vapor deposition. *Jpn. J. Appl. Phys*. **2017**, 56, 078004/1-3. https://doi.org/10.7567/JJAP.56.078004.

[19] Nishinaka, H.; Komai, H.; Tahara, D.; Arata, Y.; Yoshimoto, M. Microstructures and rotational domains in orthorhombic ε-Ga_2O_3 thin films. *Jpn. J. Appl. Phys.* **2018**, 57, 115601/1-7 https://doi.org/10.7567/JJAP.57.115601.

[20] Kracht, M.; Karg, A.; Schörmann, J.; Weinhold, M.; Zink, D.; Michel, F.; Rohnke, M.; Schowalter, M.; Gerken, B.; Rosenauer, A.; Klar, P. J.; Janek, J.; Eickhoff, M. Tin-Assisted Synthesis of ε-Ga_2O_3 by Molecular Beam Epitaxy. *Phys. Rev. Appl*. **2017**,8, 054002/1-8. https://doi.org/10.1103/PhysRevApplied.8.054002.

[21] Sun, H.; Li, K. H.; Castanedo, C. G. T.; Okur, S.; Tompa, G. S.; Salagaj, T.; Lopatin, S.; Genovese, A.; Li, X. HCl Flow-Induced Phase Change of α-; β-; and ε-Ga_2O_3 Films Grown by MOCVD. *Cryst. Growth Des*. **2018**, 18, 2370−2376. https://doi.org/10.1021/acs.cgd.7b0179.

[22] Chen, Y.; Xia, X.; Liang, H.; Abbas, Q.; Liu, Y.; Du, G. Growth Pressure Controlled Nucleation Epitaxy of Pure Phase ε- and β-Ga_2O_3 Films on Al2O3 via Metal−Organic Chemical Vapor Deposition. *Cryst. Growth Des*. **2018**, 18, 1147-1154. https://doi.org/10.1021/acs.cgd.7b01576.

[23] Zhuo, Y.; Chen, Z.; Tu, W.; Ma, X.; Pei, Y.; Wang, G. β-Ga_2O_3 versus ε-Ga_2O_3: Control of the crystal phase composition of gallium oxide thin film prepared by metal-organic chemical vapor deposition. *Applied Surface Science* **2017**, 420, 802-807. http://dx.doi.org/10.1016/j.apsusc.2017.05.241.

[24] Bosi, M.; Mazzolini, P.; Seravalli, L.; Fornari, R. Ga_2O_3 polymorphs: tailoring the epitaxial growth conditions. *J. Mater. Chem. C* **2020**, 8, 10975-10992. http://dx.doi.org/10.1039/D0TC02743J

[25] Mulazzi, M.; Reichmann, F.; Becker, A.; Klesse, W. M.; Alippi, P.; Fiorentini, V.; Parisini, A.; Bosi, M.; Fornari, R. The electronic structure of ε-Ga_2O_3; *APL Mater.* **2019**, 7, 022522/1-6. https://doi.org/10.1063/1.5054395.

[26] Kim, J.; Tahara, D.; Miura, Y.; Kim, B. G. First-principle calculations of electronic structures and polar properties of (κ;ε)-Ga_2O_3. *Appl. Phys. Express* **2018**, 11, 061101/1-4. https://doi.org/10.7567/APEX.11.061101.

[27] von Bardeleben, H. J.; Cantin, J. L.; Parisini, A.; Bosio, A.; Fornari, R. Conduction mechanism and shallow donor properties in silicon doped ε-Ga_2O_3 thin films: An electron paramagnetic resonance study. *Phys. Rev Mat*. **2019**, 3, 084601/1-8. https://doi.org/10.1103/PhysRevMaterials.3.084601.

[28] Guo, S.-D.; Du, H.-M. Piezoelectric properties of Ga_2O_3: a first-principle study. *The European Physical Journal B* **2020**, 93, 7/1-6. https://doi.org/10.1140/epjb/e2019-100516-6.

[29] Maccioni, M. B.; Fiorentini, V. Phase diagram and polarization of stable phases of $(Ga_{1-x}In_x)_2O_3$. *Appl. Phys. Express* **2016**, 9, 041102/1-4. http://doi.org/10.7567/APEX.9.041102.

[30] Pavesi, M.; Fabbri, F.; Boschi, F.; Piacentini, G.; Baraldi, A.; Bosi, M.; Gombia, E.; Parisini, A.; Fornari, R. ε-Ga_2O_3 epilayers as a material for solar-blind UV photodetectors. *Mater. Chem. Phys*. **2018**, 205, 502–507. https://doi.org/10.1016/j.matchemphys.2017.11.023.

[31] Montedoro, V.; Torres, A.; Dadgostar, S.; Jimenez, J.; Bosi, M.; Parisini, A.; Fornari, R. Cathodoluminescence of undoped and Si-doped ε-Ga_2O_3 films. *Mat Sci Eng B*. **2021**, 264, 114918/1-7. https://doi.org/10.1016/j.mseb.2020.114918.

[32] Shapenkov, S.; Vyvenko, O.; Ubyivovk, E.; Medvedev, O.; Varygin, G.; Chikiryaka, A.; Pechnikov, A.; Scheglov, M.; Stepanov, S.; Nikolaev , Halide Vapor Phase Epitaxy α- and ε-Ga_2O_3 Epitaxial Films Grown on Patterned Sapphire Substrates. *Physica Status Solidi A* **2020**, 1900892/1-6. https://doi.org/10.1002/pssa.201900892.

[33] Varley, J. B.; Peelaers, H.; Janotti, A.; Van de Walle, C. G. Hydrogenated cation vacancies in semiconducting oxides. *J. Phys.: Condens. Matter* **2011**, 23, 334212/1-9. https://doi.org/10.1088/0953-8984/23/33/334212.

[34] Lany, S. Defect phase diagram for doping of Ga_2O_3. *APL Mater*. **2018**, 6, 046103/1-9. https://doi.org/10.1063/1.5019938.

[35] von Bardeleben, H. J.; Zhou, S.; Gerstmann, U.; Skachkov, D.; Lambrecht, W. R. L.; Ho, Q. D.; Deák, P. Proton irradiation induced defects in β-Ga2O3: A combined EPR and theory study. *APL Materials* **2019**, 7, 02252/1-8. https://doi.org/10.1063/1.5053158.

[36] Skachkov, D.; Lambrecht, W. R. L.; von Bardeleben, H. J.; Gerstmann, U.; Ho, Q. D.; Deák, P. Computational identification of Ga-vacancy related electron paramagnetic resonance centers in β-Ga2O3. *Journal of Applied Physics* **2019**, 125, 185701/1-14. https://doi.org/10.1063/1.5092626.

[37] Lyons, J. L. Electronic Properties of Ga$_2$O$_3$ Polymorphs; *ECS Journal of Solid State Science and Technology*. **2019**, 8, Q3226-Q3228. https://doi.org/10.1149/2.0331907jss.

[38] Parisini, A.; Bosio, A.; Montedoro, V.; Gorreri, A.; Lamperti, A.; Bosi, M.; Garulli, G.; Vantaggio, S.; Fornari, R. Si and Sn doping of ε-Ga$_2$O$_3$ layers. *APL Mater.* **2019**, 7, 031114/1-6. https://doi.org/10.1063/1.5050982.

[39] Lyons J. L. A survey of acceptor dopants for β-Ga$_2$O$_3$. *Semicond. Sci. Technol*. **2018**, 33, 05LT02/1-5. https://doi.org/10.1088/1361-6641/aaba98.

[40] Varley, J. B.; Janotti, A.; Franchini, C.; Van de Walle, C. G. Role of self-trapping in luminescence and p-type conductivity of wide-band-gap oxides. *Phys. Rev. B* **2012**, 85, 081109. https://doi.org/10.1103/PhysRevB.85.081109

[41] Bosio, A.; Borelli, C.; Parisini, A.; Pavesi, M.; Vantaggio, S.; Fornari, R. A Metal-Oxide Contact to ε-Ga$_2$O$_3$ Epitaxial Films and Relevant Conduction Mechanism. *ECS Journal of Solid State Science and Technology; Special Issue: Focus Issue on Gallium Oxide Based Materials and Devices II; 2020 ECS J. Solid State Sci. Technol*. **2020**, 9, 055002/1-6. https://doi.org/10.1149/2162-8777/ab8f37

[42] Qin, Y.; Li, L.; Zhao, X.; Tompa, G. S.; Dong, H.; Jian, G.; He, Q.; Tan, P.; Hou, X.; Zhang, Z.; Yu, S.; Sun, H.; Xu, G.; Miao, X.; Xue, K.; Long, S.; Liu, M. Metal–Semiconductor–Metal ε-Ga$_2$O$_3$ Solar-Blind Photodetectors with a Record-High Responsivity Rejection Ratio and Their Gain Mechanism. *ACS Photonics* **2020**, 7, 812-820. https://doi.org/10.1021/acsphotonics.9b01727.

[43] Sun, H.; Li, K.-H.; Castanedo, C. G. T.; Okur, S.; Tompa, G. S.; Salagaj, T.; Lopatin, S.; Genovese, A.; Li, X. HCl Flow-Induced Phase Change of α-; β-; and ε-Ga$_2$O$_3$ Films Grown by MOCVD. *Cryst. Growth Des.* **2018**, 18, 2370-2376. https://doi.org/10.1021/acs.cgd.7b01791.

[44] Varley, J. B.; Weber, J. R.; Janotti, A.; Van de Walle, C. G. Oxygen vacancies and donor impurities in β−Ga$_2$O$_3$. *Appl. Phys. Lett.* **2010**, 97, 142106/1-3. https://doi.org/10.1063/1.3499306.

[45] Battiston, G. A.; Gerbasi, R.; Porchia, M.; Bertoncello, R.; Caccavale, F. Chemical vapour deposition and characterization of gallium oxide thin films. *Thin Solid Films* **1996**, 279, 115-118.

[46] Wei, Y.; Wang, T.; Zhang, Y.; Qi, C.; Luan, J.; Ma, G.; Tsai, H.-S.; Liu, C.; Huo, M. Effects of carbon related defects on opto-electronic properties of β-Ga2O3: The first principle calculation. *Results in Physics* **2020**, 17, 103060/1-8. https://doi.org/10.1016/j.rinp.2020.103060.

[47] Lyons, J. L.; Steiauf, D.; Janotti, A.; Van de Walle, C. G. Carbon as a Shallow Donor in Transparent Conducting Oxides. *Physical Review Applied* **2014**, 2, 064005/1-8. https://doi.org/10.1103/PhysRevApplied.2.064005.

[48] Zhang, Z.; Farzana, E.; Arehart, A. R.; Ringel, S. A. Deep level defects throughout the bandgap of (010) β-Ga$_2$O$_3$ detected by optically and thermally stimulated defect spectroscopy *Appl. Phys. Lett.* **2016**, 108, 052105/1-5. https://doi.org/10.1063/1.4941429.

[49] Irmscher, K.; Galazka, Z.; Pietsch, M.; Uecker, R.; Fornari R. Electrical properties of β-Ga₂O₃ single crystals grown by the Czochralski method. *J. Appl. Phys.* **2011**, 110, 063720/1-7. https://doi.org/10.1063/1.3642962.

[50] Ingebrigtsen, M. E.; Varley, J. B.; Kuznetsov, A. Yu.; Svensson, B. G.; Alfieri, G.; Mihaila, A.; Badstübner, U.; Vines, L. Iron and intrinsic deep level states in Ga₂O₃. *Appl. Phys. Lett*. **2018**, 112, 042104/1-5. https://doi.org/10.1063/1.5020134.

[51] Neal, A. T.; Mou, S.; Rafique, S.; Zhao, H.; Ahmadi, E.; Speck, J. S.; Stevens, K. T.; Blevins, J. D.; Thomson, D. B.; Moser, N.; Chabak, K. D.; Jessen, G. H.; Donors and deep acceptors in β-Ga₂O₃. *Appl. Phys. Lett*. **2018**, 113, 062101/1-5. https://doi.org/10.1063/1.5034474.

[52] Lenyk, C. A.; Gustafson, T. D.; Halliburton, L. E.; Giles, N. C. Deep donors and acceptors in β-Ga2O3 crystals: Determination of the $Fe^{2+/3+}$ level by a noncontact method. *J. Appl. Phys.* **2019**, 126, 245701/1-9. https://doi.org/10.1063/1.5133051.

[53] Polyakov, A. Y.; Lee, In-Hwan; Smirnov, N. B.; Yakimov, E. B.; Shchemerov, I. V.; Chernykh, A. V.; Kochkova, A. I.; Vasilev, A. A.; Ren, F.; Carey, P. H.; Pearton, S. J. Hydrogen plasma treatment of β-Ga₂O₃: Changes in electrical properties and deep trap spectra. *Appl. Phys. Lett.* **2019**, 115, 032101/1-5. https://doi.org/10.1063/1.5108790.

[54] Wei, Y.; Li, X.; Yang, J.; Liu, C.; Zhao, J.; Liu, Y.; Dong, S. Interaction between hydrogen and gallium vacancies in β-Ga₂O₃. *Scientific Reports* **2018**, 8, 10142/1-8. https://doi.org/10.1038/s41598-018-28461-3.

[55] Fleischer, M.; Giber, J.; Meixner, M. H₂-induced Changes in Electrical Conductance of β−Ga₂O₃ Thin-Film Systems. *Appl. Phys A*. **1992**, 54, 560-566

https://doi.org/10.1007/BF00324340.

[56] Li, H.; Robertson, J. Behaviour of hydrogen in wide band gap oxides. *J. Appl. Phys.* **2014**, 115, 203708/1-11. https://doi.org/10.1063/1.4878415.

[57] McCluskey, M. D.; Tarun, M. C.; Teklemichael, S. T. Hydrogen in oxide semiconductors. *J. Mater. Res.* **2012**, 27, 2190-2198. https://doi.org/10.1557/jmr.2012.137.

[58] King, P. D. C.; McKenzie, I.; Veal, T. D. Observation of shallow-donor muoniumin Ga_2O_3: Evidence for hydrogen-induced conductivity. *Appl. Phys. Lett.* **2010**, 96, 062110/1-3. https://doi.org/10.1063/1.3309694.

[59] Kim, J.; Pearton, S. J.; Fares, C.; Yang, J.; Ren, F.; Kima, S.; Polyakov, A. Y. Radiation damage effects in Ga_2O_3 materials and devices. *J. Mater. Chem. C* **2019**, 7, 10-24. https://doi.org/10.1039/c8tc04193h.

[60] Son, N. T.; Goto, K.; Nomura, K.; Thieu, Q. T.; Togashi, R.; Murakami, H.; Kumagai, Y.; Kuramata, A.; Higashiwaki, M.; Koukitu, A.; Yamakoshi, S.; Monemar, B.; Janzén, E. Electronic properties of the residual donor in unintentionally doped $\beta-Ga_2O_3$. *J. Appl. Phys.* **2016**, 120, 235703/1-3. https://doi.org/10.1063/1.4972040.

[61] Lannoo, M.; Bourgoin, J. *Point Defects in Semiconductors*; Springer Series in Solid-State Sciences book series vol. 22 (I: Theoretical Aspects) and 35 (II: Experimental Aspects); Springer-Verlag Berlin Heidelberg, **1981**; Series Print ISSN 0171-1873 https://doi.org/10.1007/978-3-642-81574-4 and https://doi.org/10.1007/978-3-642-81832-5

[62] Swallow, J. E. N.; Varley, J. B.; Jones, L. A. H.; Gibbon, J. T.; Piper, L. F. J.; Dhanak, V. R.; Veal, T. D. Transition from electron accumulation to depletion at $\beta-Ga_2O_3$ surfaces: The role

of hydrogen and the charge neutrality level. *APL Mater*. **2019**, 7, 022528/1-8. https://doi.org/10.1063/1.5054091.

[63] Tadjer, M. J.; Koehler, A. D.; Freitas, J. A.; Gallagher, J. C.; Specht, M. C.; Glaser, E. R.; Hobart, K. D.; Anderson, T. J.; Kub, F. J.; Thieu, Q. T.; Sasaki, K.; Wakimoto, D.; Goto, K.; Watanabe, S.; Kuramata, A. High resistivity halide vapor phase homoepitaxial β-Ga$_2$O$_3$ films co-doped by silicon and nitrogen. *Appl. Phys. Lett.* **2018**, 113, 192102/1-5. https://doi.org/10.1063/1.5045601.

[64] Peelaers, H.; Lyons, J. L.; Varley, J. B.; Van de Walle, C. G. Deep acceptors and their diffusion in Ga$_2$O$_3$. *APL Mater*. **2019**, 7, 022519/1-6. https://doi.org/10.1063/1.5063807.

[65] Gao, H.; Muralidharan, S.; Pronin, N.; Karim, M. R.; White, S. M.; Asel, T.; Foster, G.; Krishnamoorthy, S.; Rajan, S.; Cao, L. R.; Higashiwaki, M.; von Wenckstern, H.; Grundmann, M.; Zhao, H.; Look, D. C.; Brillson, L. J. Optical signatures of deep level defects in Ga$_2$O$_3$. *Appl. Phys. Lett.* **2018**, 112, 242102/1-5. https://doi.org/10.1063/1.5026770.

[66] Mott, N. F. *Metal-insulator transitions* Taylor and Francis Ltd ISBN 0-85066-783-6, **1990**.

[67] Shklovskii, B. I.; Efros, A. L. *Electronic Properties of Doped Semiconductors* Springer Verlag Solid-State Science 45 ISBN 3-540-12995-2, **1984**.

[68] Altermatt, P. P.; Schenk, A.; Heiser, G. A simulation model for the density of states and for incomplete ionization in crystalline silicon. I. Establishing the model in Si:P. *J. Appl. Phys.* **2006**, 100, 113714/1-10. http://dx.doi.org/10.1063/1.2386934.

[69] Bosio, A.; Parisini, A.; Lamperti, A.; Borelli, C.; Fornasini, L.; Bosi, M.; Cora, I.; Fogarassy, Z.; Pécz, B.; Zolnai, Z.; Németh, A.; Vantaggio, S.; Fornari, R. *n*-Type Doping of ε-

Ga$_2$O$_3$ Epilayers by High-Temperature Tin Diffusion. **2021** Available at SSRN: https://ssrn.com/abstract=3757760 or http://dx.doi.org/10.2139/ssrn.3757760.

[70] Nikolaev, V. I.; Stepanov, S. I.; Pechnikov, A. I.; Shapenkov, S.V.; Scheglov, M. P.; Chikiryaka, A.V.; Vyvenko, O. F. HVPE Growth and Characterization of ε-Ga2O3 Films on Various Substrates. *ECS Journal of Solid State Science and Technology* **2020**, 9, 045014/1-6. https://doi.org/10.1149/2162-8777/ab8b4c.

[71] Cai, Y.; Zhang, K.; Feng, Q.; Zuo, Y.; Hu, Z.; Feng, Z.; Zhou, H.; Lu, X.; Zhang, C.; Tang, W.; Zhang, J.; Hao, Y. Tin-assisted growth of ε-Ga$_2$O$_3$ film and the fabrication of photodetectors on sapphire substrate by PLD. *Optical Materials Express* **2018**, 8, 3506/1-12. https://doi.org/10.1364/OME.8.003506.

[72] Kneiß, M.; Hassa, A.; Splith, D.; Sturm, C.; von Wenckstern, H.; Lorenz, M.; Grundmann, M. Epitaxial stabilization of single phase κ-(In$_x$Ga$_{1-x}$)$_2$O$_3$ thin films up to x = 0.28 on c-sapphire and κ-Ga$_2$O$_3$(001) templates by tin-assisted VCCS-PLD. *APL Mater.* **2019**, 7, 101102/1-10. https://doi.org/10.1063/1.5120578.

[73] Parisini, A.; Fornari R. Analysis of the scattering mechanisms controlling electron mobility in β-Ga$_2$O$_3$ crystals. *Semicond. Sci. Technol.* **2016**, 31, 035023/1-16. https://doi.org/10.1088/0268-1242/31/3/035023-

[74] Parisini, A.; Ghosh, K; Singisetti, U.; Fornari, R. Assessment of phonon scattering-related mobility in β-Ga$_2$O$_3$. *Semicond. Sci. Technol.* **2018**, 33, 105008/1-9, https://doi.org/10.1088/1361-6641/aad5cd.

[75] Korhonen, E.; Tuomisto, F.; Gogova, D.; Wagner, G.; Baldini, M.; Galazka, Z.; Schewski, R.; Albrecht, M. Electrical compensation by Ga vacancies in Ga_2O_3 thin films. *Applied Physics Letters* **2015**, 106, 242103/1-3. https://doi.org/10.1063/1.4922814.

AUTHOR INFORMATION

Corresponding Author

*Antonella Parisini, antonella.parisini@unipr.it University of Parma, Department of Mathematical, Physical and Computer Sciences, Parco Area delle Scienze 7/A, 43124 Parma, Italy

Author Contributions

The manuscript was written through contributions of all authors. All authors have given approval to the final version of the manuscript.